MATERIALE PLASTICE
https://revmaterialeplastice.ro
https://doi.org/10.37358/Mat.Plast.1964

The Strain Sensoring Behavior of the Melt-extruded Ethylene-vinyl Acetate (EVA)/carbon Black Composites Filament

SHA LI[1], WEI GAO[1], QIANG ZHANG[1,2], ZHENGSHUAI JIANG[1], LEI CHEN[3*]
[1]School of Mechanical Engineering, Shangqiu Institute of Technology, Middle Section of Suiyang Avenue No. 236, Shangqiu 476000, China
[2]College of Materials and Metallurgy, Guizhou University, South Section of Huaxi Avenue No. 2708, Guizhou 550000, China
[3]School of Software, Henan University, Jinming road No. 85, Kaifeng 475001, China

Abstract**:** *In this study, Ethylene-vinyl acetate (EVA) based composites filament, with four different volume fraction of the nano-sized carbon black particles (NCB) were produced by melt mixing using a single extruder. The morphology of the EVA/NCB was studied using SEM, where a 3-D network of the NCB was presented. Thermal gravity analysis (TGA) measurement was utilized, denoting the degradation temperature of EVA, and presetting the actual volume fraction of NCB in the composites. Mechanical properties, e.g. elongation at break, tensile strength of the EVA/NCB filament was studied. Most importantly, the strain sensoring behavior of the EVA/NCB was investigated ultilizing a tensile testing machine coupled with a pico-ammeter. The gauge factor for various strain range, as well as the relative change of the resistance during the cyclic measurement of the NCB/EVA composites was calculated. Moreover, the measured data were fitted using some mathematical modellings, which reveals the potential of the strain sensoring behavior of the NCB/EVA composites in this study. Overall, this study introduces a durable NCB/EVA composites using as strain sensor oriented to industrial large-scale production, and the proposed modelling provides an effective evaluation method on its strain sensoring behavior.*

Keywords*: EVA, carbon black, electrical conductivity, strain sensoring*

1. Introduction

Nowadays, Conductive Polymeric Composites (CPCs) have been widely studied around the world [1-6]. The advantages of the CPCs are quite remarkable, e.g. great possibility of continuous industrial production [7-9], enhanced mechanical properties comparing to the neat polymer [10], the additional electrical conductivity [11, 12] etc. The basic components of the CPCs are (1) the polymeric matrix, which endows the basic mechanical properties of the CPCs, and (2) the functionalized conductive particles, which forms conductive network in the composites, and thus provides the designed function to the matrix, i.e. the CPCs [13]. In this case, the choice of the polymeric matrix could be multifarious, aiming at various desired application of the composites. For instance, flexible polymer (e.g. poly(dimethylsiloxane) (PDMS) [14-16] and thermoplastic polyurethane (TPU) [17-20]),) have been widely employed for the preparation of the flexible CPCs, which are able to provide a great stretchability and an outstanding recoverability of the CPCs [21-25]. Moreover, under the externally applied strain on the CPC, the deformation of the conductive network of the conductive particles in the composites results in a real-time change of the resistance of the CPCs [26-28]. This is the fundamental principle of CPC-based strain sensors, which have been widely applied in human motion detection, human-computer interaction and other intelligent fields [29].

Ethylene-vinyl acetate (EVA) is the copolymer of ethylene and vinyl acetate, which is elastomeric "rubber-like" in softness and flexibility [30-33]. Besides, by adjusting the proportion between the ethylene and vinyl acetate, the dominated amorphous part in the semi-crystalline structure of EVA could be designed and achieved [34, 35]. This means the effect of the crystallization of the EVA could be

**email: leichensq@yeah.net*

ignored, which realizes a great dispersion of the fillers during the preparation as well as during its service life. Nano-sized carbon black is a common filler used in plastics to achieve conductivity [36-38], which is, not only low in cost, but also easy to disperse in the matrix due to its 0-dimentrional spherical geometry [39-41].

Processing and the mechanical properties of EVA-based composite have been investigated. Soumya Mondal et al. [42] reveals the influence of different methods of CB incorporation in the compatible blend of 50/50 (wt. %) EVA and acrylonitrile butadiene elastomer (NBR) on different properties of vulcanized blend compounds. Haohao Lu et al. [43] prepared the flexible and intelligent CFF/EVA EMI shielding composites with electrothermal-driven shape memory performance by hot-pressing method, which provide precise and convenient control-method for driving EMI shielding conversion. As revealed, the CFF/EVA composites can achieve an EMI shielding effect of 45.6 dB in X-band and maintain a ca. 99% shape memory recovery ratio. Moreover, the composites can quickly return to the original shape at low voltage, and realize accurate and fast remote emergency control EMI shielding. Felicia Stan et al. [44] investigated the rheological properties of EVA filled with various contents (0.1-5 wt. %) of multi-walled carbon nanotubes (MWCNTs) using a capillary rheometer at temperatures and shear rates relevant to the injection molding process. Yumeng Wang et al. [45] reported a stretchable and compressible conductive foam with stable mechano-electrical properties comprised of copper nanowires and MWCNTs that were wrapped firmly on flame-retardant EVA skeleton. Zishou Zhang et al. [46] developed a highly conductive and lightweight membrane substrate based on EVA, CNTs and lens wiping paper, and demonstrated its implementation as high-performance mechanical support for MnO_2 in supercapacitors.

However, to the best of our knowledge, the nano-sized CB have been rarely reported to produce EVA based composite. Since the NCB particles enables the flexible EVA composites electrical conductivity, its potential of strain sensoring behavior should be in depth investigated and revealed.

2. Materials and methods

2.1. Preparation of EVA/NCB composite filament

The EVA copolymer used in study was obtained as Elvax 265 from DuPont, with a VA content of 28% and MFI of 3. Conductive CB particles were provided by Orion Engineered Carbons Co., Ltd. Both the polymer granules and the CB powder were dried at 60ºC for 48h in a vacuum oven to completely remove the moisture. Afterwards, both raw materials with the designed ratio were simultaneously fed into a co-rotating twinscrew extruder (Leistritz Micro-18/GL-40D) at 60 rpm at 120ºC, equipping with a die with diameter of 3mm. All the extruded composite filament was firstly pelletized and then fed back to the same extruder at 60 rpm at 120ºC for the second time, but with die with diameter of 1 mm, to produce the final desired EVA/NCB composite filaments. The filament was then cut into specimen with a length of 4 cm for further measurements.

2.2. Characterization

The morphologies of the EVA/CB composites were studied by a scanning electron microscope (ZEISS EVO). The specimens were sputtered with a thin layer of gold, then were analyzed with a secondary electron detector at an acceleration voltage of 10 kV.

The thermal stability of specimens was tested using Thermogravimetric Analysis (TGA) (TA Instruments, 2960) from room temperature to 1000ºC at a heating rate of 10ºC /min under nitrogen atmosphere. The electromechanical properties of the samples were investigated on a tensile testing machine (Zwick, Z005) coupled with a Keithley 6485 Picoammeter. As shown in Figure 1, specimens were fixed on the tensile testing machine with gauge length of 20 mm. Several layers of isolated tapes were employed to encase the clapper of the testing machine. For the dynamic resistance measurement during stretching, a strain rate of 60 mm/min was applied onto the specimens. In the dynamic electromechanical measurement at least 10 specimens were tested and in the cyclic strain sensing test the data of at least 5 specimens were recorded for each experiment. Following nomenclature was applied

for the description of all the samples in this study: ***CB5*** denotes the designed volume fraction of the NCB in the composite is 5 vol. %, and ***Virgin*** denotes the neat EVA polymer extruded using the twin extruder under same condition as a contrast.

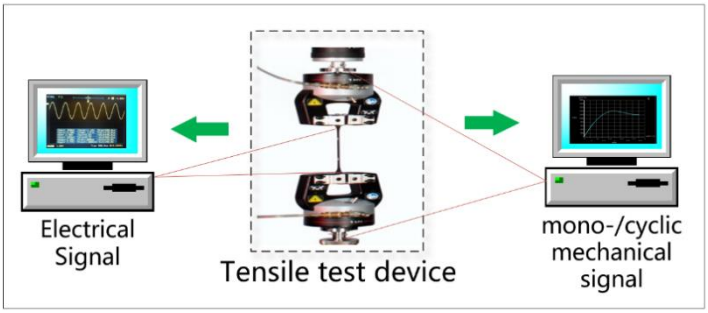

Figure 1. The tensile test machine coupled with the ammeter to record strain and resistance data during stretching

3. Results and discussions

3.1. Morphologies

The cross section microstructures of stretched EVA/CB composite filament were investigated using SEM as shown in Figure 2. An obvious phase separation between the EVA/CB, which are NOT participated into the stretching process (red region in the Figure 2a) is observed. This indicates the inhomogeneous dispersion of the EVA matrix from each other using the single extruder, which would be improved by increasing the kneading time using a twin extruder. However, the zoomed in region of the damaged region of the EVA/CB region still shows a great dispersion of the CB particle in the EVA matrix, which was attributed from the two-step melting mixing during the preparation process.

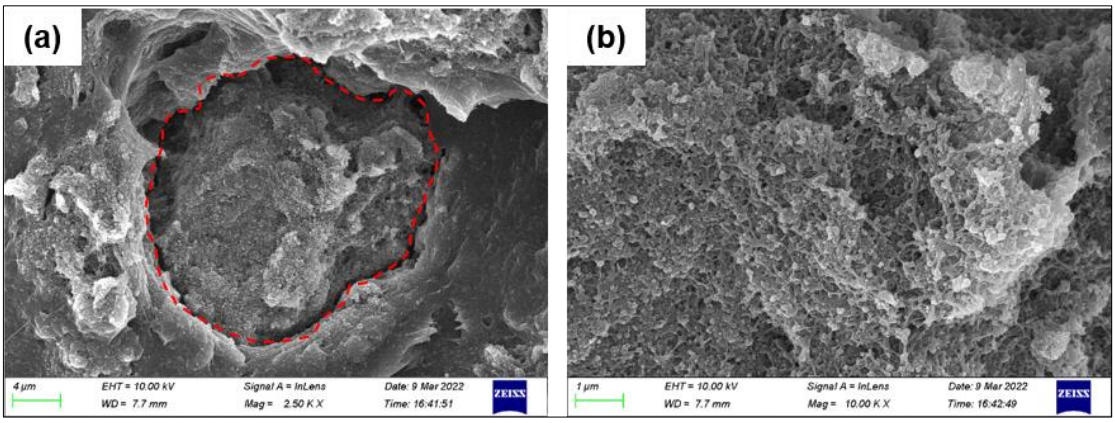

Figure 2. SEM pictures of cross section of the EVA/CB composite filament in this study

3.2. Thermal gravity analysis

Figure 3 shows the TGA measurements of EVA/CB composite filaments, where the remained mass of all the specimen versus temperature are presented in different colors. It should be noted that the weight reduction of all the samples starts firstly at approximately 300°C (degradation temperature of EVA), which indicates a temperature range for practical applications of the composites. The weight percentage of the sample remains stable after 600°C, indicating the remaining composition in the sample after heat treatment. The inserted value denoted the final remained weight of the samples, tie difference between which and the remained mass of the Virgin (8%) denotes the real weight fraction of the CB in the sample. For instance, the real weight fraction of the 5CB can be calculated as 13.6 % - 8.0 %=5.6 %.

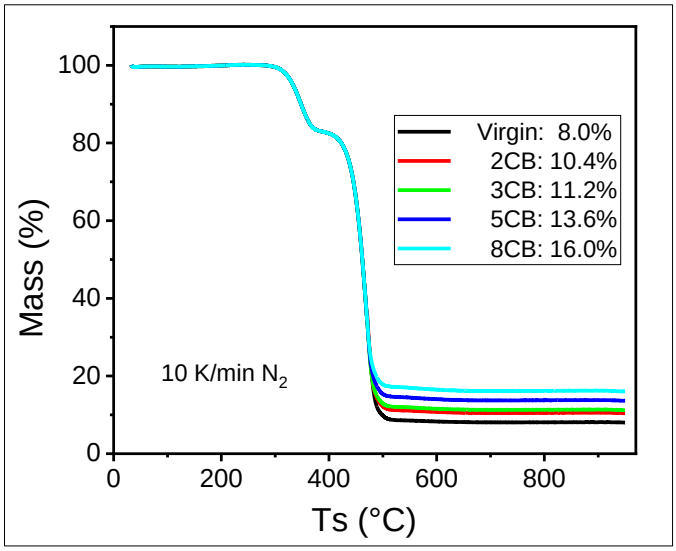

Figure 3. The weight fraction of the samples versus the temperature in order to obtain the thermal behavior and the real weight fraction of the composites

3.3. Mechanical properties

The stress-strain curves of all the investigated five samples obtained from the tensile testing machine are shown in Figure 4. It should be noted that the strain range of the EVA/CB composite filament presents a low range despite of its great flexibility. This is because the phase separation between the EVA matrix during the melt mixing process, as shown in Figure 2a. The composite filament with 2% and 3% CB shows an increased elongation at break comparing to that of the virgin EVA, but filament with more than 5% CB shows a decreased elongation at break comparing to that of the virgin EVA. This is because the addition of the CB particles hinders the construction of the continuous phase of the polymeric matrix, resulting in a lower elongation at break.

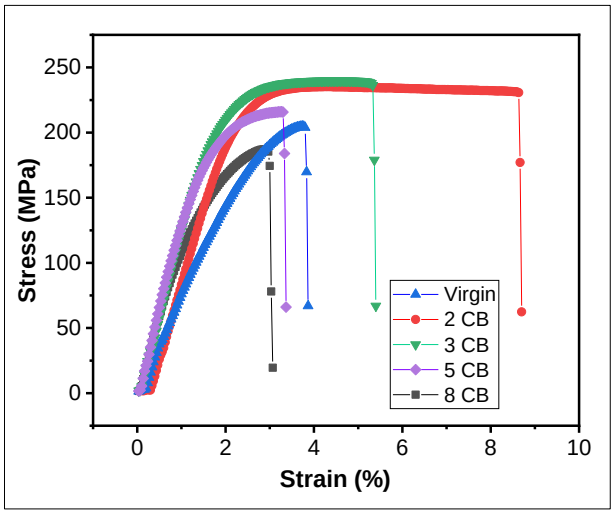

Figure 4. Stress-Strain curve of the investigated EVA/CB composite filaments in this study

The Young's modulus of the samples was calculated using the first 15 points of the stress-strain curve of each sample, and presented in Figure 5 in blue. We can see that as the content of CB increases, the Young's modulus of the samples is significantly improved, which was attributed to the higher fraction of CB in the samples during the linear elastic deformation region of the samples.

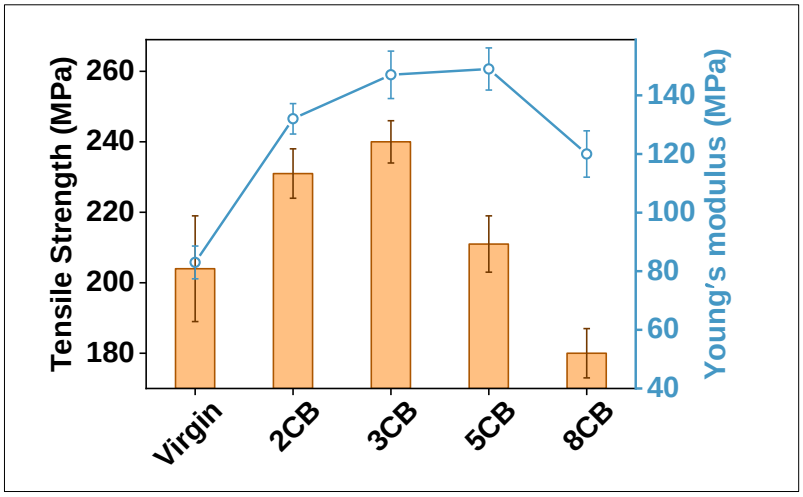

Figure 5. Diagram of the Young's modulus (right axis, data in blue) and the tensile strength (left axis, data in orange) versus different fraction of the carbon black in the composite filaments

3.4. Electrical conductivity

As the contents of the CB fillers increases in the EVA composites, the electrical conductivity of which also increases. The percolation threshold is usually applied to describe a critical volume fraction of the conductivity fillers, where the conductivity of the composites increases fastest. An equation proposed by McLachlan is often used to compute the percolation threshold for conductive composites [47]:

$$(1-\phi)\frac{{\sigma_m}^{1/s}-{\sigma_c}^{1/s}}{{\sigma_m}^{1/s}+{\sigma_c}^{1/s}(1-\phi_c)/\phi_c}+\phi\frac{{\sigma_f}^{1/t}-{\sigma_c}^{1/t}}{{\sigma_f}^{1/t}+\frac{1-\phi_c}{\phi_c}\cdot{\sigma_c}^{1/t}}=0 \quad (1)$$

where $\sigma_m, \sigma_c, \sigma_f$ denotes the conductivity of the EVA matrix, the EVA/CB composite, and the CB, respectively. ϕ is the volume fraction of the CB and ϕ_c is the critical volume concentration, i.e. the percolation threshold. The standard value of the exponent t is 0.87. For isotropic composites with randomly oriented fillers, the standard value of the exponent s is 2. However, in this study s was set to 1.5, because the CB distribution was not isotropic. The value of ϕ_c was calculated to 3.1 %, using equation 1.

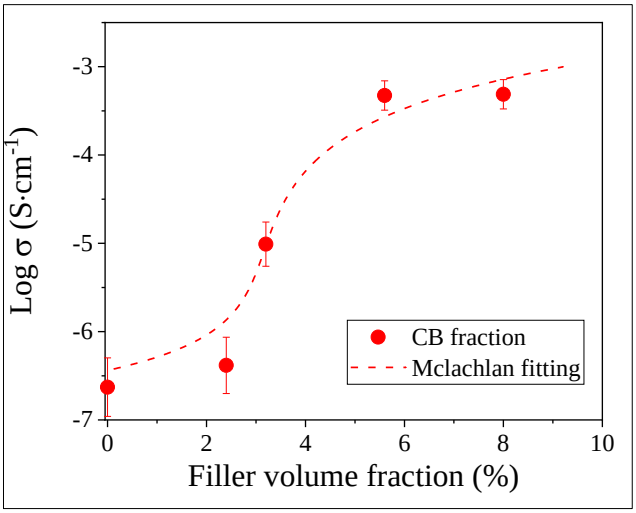

Figure 6. Electrical conductivity of the EVA/CB composites filament as a function of the volume fraction of CB, fitting with McLachlan equation (dashed line)

3.5. Uniaxial strain sensing behavior

The relative change in resistance (RCR) of an electrically conductive composite was expressed as:

$$RCR = \frac{\Delta R}{R_0} = \frac{R - R_0}{R_0} \tag{2}$$

where the ΔR, R_0, and R denotes the change of the resistance, the initial resistance, and the resistance under strain in time, respectively. Figure 9 presents the RCR value of all the specimen versus applied strain in different color.

Gauge factor (*GF*), which is generally defined as the ratio of relative resistance with applied strain as shown in equation 3, and is used to reveal the sensitivity of the strain sensor [48].

$$GF = \frac{d(RCR)}{d\varepsilon} = \frac{d[(R(t) - R_0)/R_0]}{d\varepsilon} \tag{3}$$

where *RCR* denotes the relative change of the resistance, R_t and R_0 is the real-time resistance during stretching and the initial resistance before stretching of the NCB/EVA, respectively. $\boldsymbol{\varepsilon}$ denotes the external strain in percentage. The GF value of each specimen for differnet region was marked in dashed line in Figure 7.

The measurable strain response range was between 2% to 5% for all the specimens. The minimum GF was about 4, and the maximum GF of all the specimen was found in the higher applied range of ***2CB*** about 112. Generally, the GF value of specimen with lower CB contents is higher than that with the higher CB contents. This is because the composites with higher CB content contains a stable 3-D conductive network, which is not effectively effected by the deformation of the polymeric matrix.

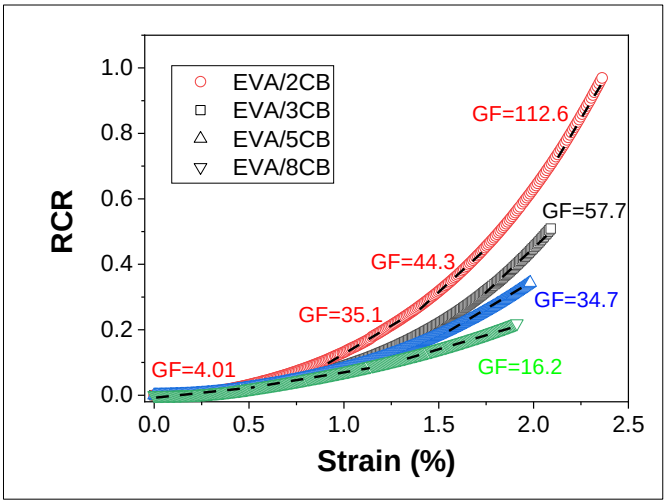

Figure 7. Relative change in resistivity (RCR) as a function of applied strain for all the composites filament in the study, gauge factors (GF) are marked using dashed lines

The relationship between the microscopic structure of the nano particles and the macroscopic electromechanical properties of the CPCs under external loading have been widely reported [49]:

$$R = \frac{L}{N} R_m = \frac{L}{N}\left(\frac{8\pi hs}{3\gamma a^2 e^2}\right) exp(\gamma s) \tag{4}$$

where L is the length of particles forming on conducting pathway, N is the number of conducting pathways, R_m is the resistance between two adjacent particles, h is Plank's constant, a^2 is the effective cross-sectional area, e is the electron charge,

$$\gamma = \frac{4\pi\sqrt{2m\varphi}}{h} \tag{5}$$

where m is the electron mass, $\boldsymbol{\varphi}$ is the height of the potential barrier between the adjacent particles and s is the shortest distance between adjacent conductive particles. When the applied strain is uniaxial, the separation s between adjacent conductive particles can be given by:

$$s(\varepsilon) = s(0)(1 + C\varepsilon) \tag{6}$$

where C is constant, and $s(0)$ is the initial distance between adjacent particles. Moreover, the number of conducting paths N in real time can be predicted as:

$$N(\varepsilon) = \frac{N(0)}{exp(M\varepsilon + W\varepsilon^2 + U\varepsilon^3 + V\varepsilon^4)} \tag{7}$$

where M, W, U, V are all fitting parameters. The distance between both adjacent particles is assumed to be synchronously changed from $s(0)$ to $s(\varepsilon)$ and the number of conducting paths varying from $N(0)$ to $N(\varepsilon)$, then the relative change of the resistance (RCR) is expressed by:

$$\frac{\Delta R}{R_0} = \frac{R - R_0}{R_0} = \frac{s(\varepsilon)/N(\varepsilon)}{s(0)/N(0)} exp\{\gamma[s(\varepsilon) - s(0)]\} - 1 \tag{8}$$

Substituting equation 6 and equation 7 into equation 8 yields:

$$\frac{\Delta R}{R_0} = (1 + C\varepsilon)exp[(M + \gamma s(0)C)\varepsilon + W\varepsilon^2 + U\varepsilon^3 + V\varepsilon^4] - 1 \tag{9}$$

The data from Figure 6 was fitted using equation 9 and presented in Figure 7 with corresponding color. The promising fitting results indicates the success of the modelling, and the great potential of the EVA/CB composites filaments in strain sensoring application.

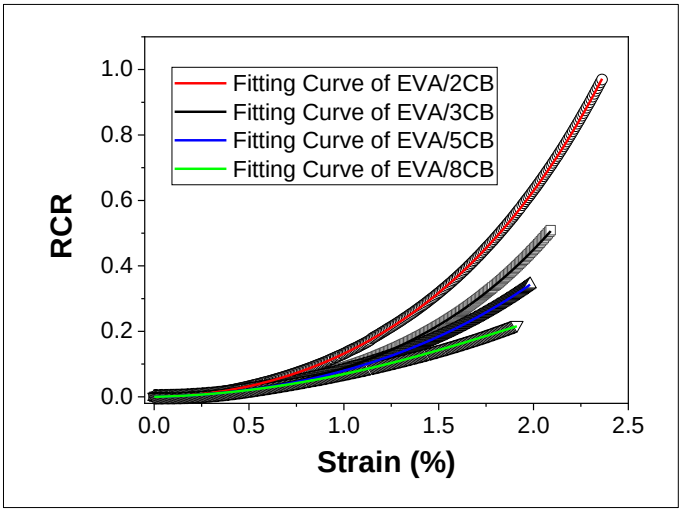

Figure 8. RCR value as a function of strain of using the data points, the fitting results using equation 9 are displayed using curves in different colors

3.6. Cyclic strain sensing behavior

The RCR value of specimen *5CB* and *2CB* as a function of time under a strain of 1% during cyclic tests were presented in Figure 8 in blue and red, respectively. Ten cycles of values were displayed, where a great periodicity of both filaments were observed (10 output peaks). Furthermore, two dashed lines were given for a better comparison between the input strain signal and the output electrical signal. According to which, hardly any delayed signal between the input and the output signal derived from the EVA composites were found. This denotes a great repeatability and superior recoverability of the EVA-based composites.

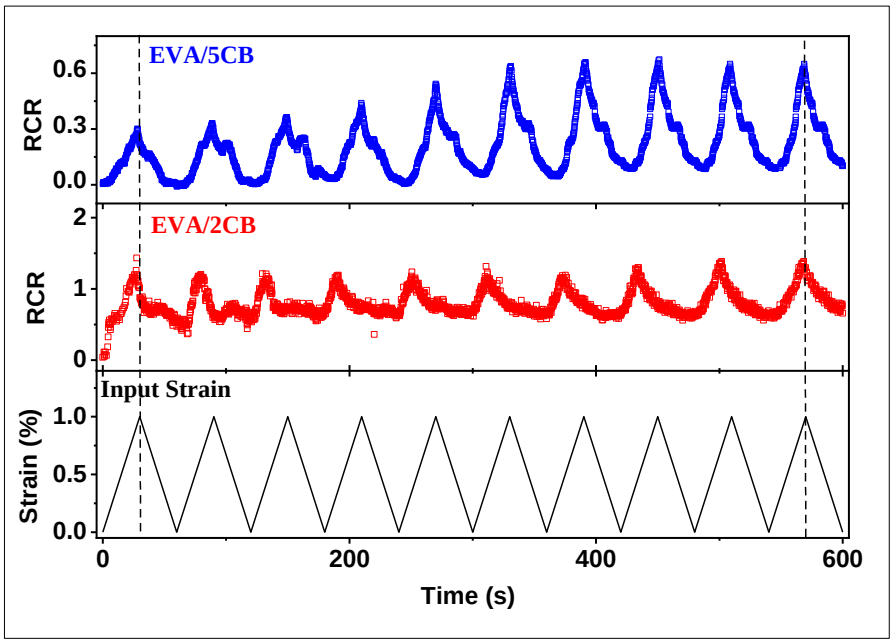

Figure 9. RCR value versus time for EVA/5CB (blue) and ***EAV/2CB*** (red), under 10 cycles of stretching, respectively

In addition, several single data points were detected for the specimen *EVA/2CB*, which can be treated as noise during the measurement and can be ignored using algorithm for the application. Besides, an obvious shoulder peak can be found in the RCR value of the *EVA/5CB* specimen. This is a common phenomenon for the melt-mixed composites, as reported in [50]. In this study, however, only the EVA-based composites with high fraction of CB presents the "shoulder-peak" feature. Thus, a diagrammatic sketch was presented in Figure 10 to offer a hypothetical explanation.

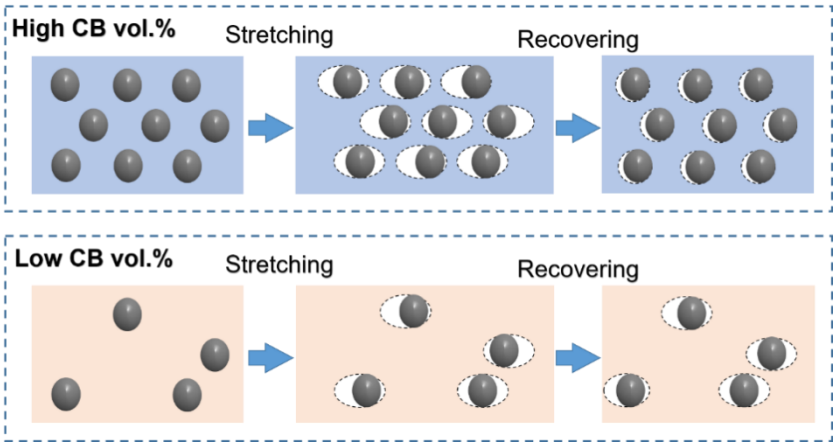

Fig. 10 Diagrammatic sketch for the change of the created cavity EVA/CB composites during stretching

During the stretching process, the EVA matrix was uniformly elongated along the stretching direction, the rigid CB particles remain unchanged and embedded in the created cavities as the dashed ellipse. The cavities shrink back during the recovering process, which complete a cycle during cyclic test. However, the higher fraction of CB (in blue) endows a higher steric resistance, which hinder the recoverability of the created cavities. Therefore, the recovering process of the matrix contains an extra recovering process due to the rigid CB particles, resulting into the shoulder peak in the RCR diagram comparing to the composites with a lower fraction of CB particles.

4. Conclusions

In this study, NCB/EVA composites filament with four different NCB fraction were produced. The morphological study as well as a TGA measurement was utilized to present the structure and content of the NCB particles in the composites, respectively.

Comparing to the others, the specimen EVA/2CB presents the highest elongation at break, acceptable Tensile strength and the Young`s modulus. The percolation threshold of the EVA/CB composites was revealed as 3.1% by fitting the Mclachlan equation. The relative change in resistivity (RCR) as a function of applied strain for all the composites filament were presented, where all the GF value was calculated. Moreover, the strain sensoring behavior was successfully fitted by the modelling derived from the tunneling theory. The cyclic strain sensing behavior was also investigated, where a sketch based on the steric resistance of the CB particles was suggested to explain the shoulder peak phenomena. Overall, this study presents a fundamental investigation on the electrical and mechanical behavior of the EVA/NCB composites filament, which provides some guidance of the sensoring application based on the mass industrial production.

Acknowledgement: The authors would like to thank the financial support from the National Natural Science Foundation of China under Grants 11875183, and Henan Provincial Science and Technology Research Project under Grants 222102210141, Henan Provincial Natural Science Foundation of China (212102210221).

References

1. LI W, HAN C, ZHANG K, et al., Strategies for boosting carbon electrocatalysts for the oxygen reduction reaction in non-aqueous metal–air battery systems[J]. Journal of Materials Chemistry A, 2021, 9(11): 6671-6693.
2. NG B, FAEGH E, LATEEF S, et al., Structure and chemistry of the solid electrolyte interphase (SEI) on a high capacity conversion-based anode: NiO[J]. Journal of Materials Chemistry A, 2021, 9(1): 523-537.
3.LIU H, GAO H, HU G., Highly sensitive natural rubber/pristine graphene strain sensor prepared by a simple method[J]. Composites, 2019, 171(AUG.15):138-145.
4. ZHAO S, X MENG, LIU L, et al., Polypyrrole-coated copper nanowire-threaded silver nanoflowers for wearable strain sensors with high sensing performance[J]. Chemical Engineering Journal, 2020, 417:127966.
5.*** Using Stretchable PPy@PVA Composites as a High-Sensitivity Strain Sensor to Monitor Min Motion[J]. ACS Applied Materials and Interfaces, 2020, 12(40):45373-45382.
6. HE, Y., WU, D., ZHOU, M., ZHENG, Y., WANG, T., LU, C., ... LIU, C., (2021), Wearable strain sensors based on a porous polydimethylsiloxane hybrid with carbon nanotubes and graphene. ACS Applied Materials & Interfaces, 13(13), 15572-15583.
7. WU, L., LI, L., PAN, L., WANG, H., BIN, Y., (2021), MWCNTs reinforced conductive, self-healing polyvinyl alcohol/carboxymethyl chitosan/oxidized sodium alginate hydrogel as the strain sensor. Journal of Applied Polymer Science, 138(6), 49800.

8. SUN, X., QIN, Z., YE, L., ZHANG, H., YU, Q., WU, X., ... Yao, F., (2020), Carbon nanotubes reinforced hydrogel as flexible strain sensors with high stretchability and mechanically toughness. Chemical Engineering Journal, 382, 122832.
9. CHANG, K., LI, M., ZHONG, W., WU, Y., LUO, M., CHEN, Y., ... WANG, D., (2019), A novel, stretchable, silver-coated polyolefin elastomer nanofiber membrane for strain sensor applications. Journal of Applied Polymer Science, 136(36), 47928.
10. KIM, I., WOO, K., ZHONG, Z., KO, P., JANG, Y., JUNG, M., ... MOON, J., (2018), A photonic sintering derived Ag flake/nanoparticle-based highly sensitive stretchable strain sensors for human motion monitoring. Nanoscale, 10(17), 7890-7897.
11. LIU, H., LI, Q., ZHANG, S., YIN, R., LIU, X., HE, Y., ... GUO, Z., (2018), Electrically conductive polymer composites for smart flexible strain sensors: a critical review. Journal of Materials Chemistry C, 6(45), 12121-12141.
12. QU, M., QIN, Y., SUN, Y., XU, H., SCHUBERT, D. W., ZHENG, K., ... NILSSON, F., (2020), Biocompatible, flexible strain sensors fabricated with polydopamine-coated nanocomposites of nitrile rubber and carbon black. ACS Applied Materials & Interfaces, 12(37), 42140-42152.
13. JYOTI, J., BASU, S., SINGH, B. P., DHAKATE, S. R., (2015), Superior mechanical and electrical properties of multiwall carbon nanotube reinforced acrylonitrile butadiene styrene high performance composites. Composites Part B: Engineering, 83, 58-65.
14.MONTAZERIAN H, DALILI A, MILANI A S, et al., Piezoresistive sensing in chopped carbon fiber embedded PDMS yarns[J]. Composites Part B Engineering, 2019, 164.
15.WANG L, CHEN Y, LIN L, et al., Highly stretchable, anti-corrosive and wearable strain sensors based on the PDMS/CNTs decorated elastomer nanofiber composite[J]. Chemical Engineering Journal, 2019, 362:89-98.
16. CHEN, J., ZHU, Y., JIANG, W., (2020), A stretchable and transparent strain sensor based on sandwich-like PDMS/CNTs/PDMS composite containing an ultrathin conductive CNT layer. Composites Science and Technology, 186, 107938.
17. LEPAK-KUC S, PODSIADY B, SKALSKI A, et al., Highly Conductive Carbon Nanotube-Thermoplastic Polyurethane Nanocomposite for Smart Clothing Applications and Beyond[J]. Nanomaterials, 2019, 9(9):1287.
18. HU X, TIAN M, XU T, et al., Multiscale Disordered Porous Fibers for Self-Sensing and Self-Cooling Integrated Smart Sportswear[J]. 2019.
19. JP A, BH A, WS B, et al., Highly sensitive and durable wearable strain sensors from a core-sheath nanocomposite yarn - ScienceDirect[J]. Composites Part B: Engineering, 183.
20. XU, X., WANG, T., (2018), Electrical and rheological properties of carbon black and carbon fiber filled low-density polyethylene/ethylene vinyl acetate composites. Science and Engineering of Composite Materials, 25(4), 715-723.
21. PADHI, S., PARIDA, S., SAHOO, P. K., NAIK, B., PARIDA, B. N., NAYAK, N. C., (2021), Dielectric behaviour of EVA/EPDM/HNT ternary nanocomposites. Materials Today: Proceedings, 41, 211-215.
22. LIU, J., HE, Y., CHANG, H., GUO, Y., LI, H., PAN, B., (2020), Simultaneously improving flame retardancy, water and acid resistance of ethylene vinyl acetate copolymer by introducing magnesium hydroxide/red phosphorus co-microcapsule and carbon nanotube. Polymer Degradation and Stability, 171, 109051.
23. CZANIKOVÁ, K., TORRAS, N., ESTEVE, J., KRUPA, I., KASÁK, P., PAVLOVA, E., ... Omastová, M., (2013), Nanocomposite photoactuators based on an ethylene vinyl acetate copolymer filled with carbon nanotubes. Sensors and Actuators B: Chemical, 186, 701-710.
24. CHAI, F., WANG, G., LIU, F., JIANG, D., YAO, C., XU, T., DAI, Y., (2020), Preparation and properties of flame-retardant neutron shielding material based on EVA polymer reinforced by radiation modification. Radiation Physics and Chemistry, 174, 108984.

25. LI, S. N., LI, Z. M., YANG, M. B., HU, Z. Q., XU, X. B., HUANG, R., (2004), Carbon nanotubes induced nonisothermal crystallization of ethylene–vinyl acetate copolymer. Materials Letters, 58(30), 3967-3970.
26. LIU, C. M., MA, F. F., ZHANG, Z. X., YANG, J. H., WANG, Y., ZHOU, Z. W., (2016), Enhanced tensile creep stability of immiscible poly (l-lactide)/poly (ethylene vinyl acetate) blends achieved by adding carbon nanotubes. Composites Part B: Engineering, 107, 174-181.
27. MONDAL, R. K., DUBEY, K. A., PRAKASH, S. B., KUMAR, J., MELO, J. S., BHARDWAJ, Y. K., (2021), Copolymer composition tailored carbon nanotube network breakdown and piezoresistivity of ethylene-vinyl acetate electroconductive composites. Materials Science and Engineering: B, 270, 115194.
28. SHI, Y. Y., YANG, J. H., HUANG, T., ZHANG, N., CHEN, C., WANG, Y., (2013), Selective localization of carbon nanotubes at the interface of poly (L-lactide)/ethylene-co-vinyl acetate resulting in lowered electrical resistivity. Composites Part B: Engineering, 55, 463-469.
29. VAHABI, H., GHOLAMI, F., KARASEVA, V., LAOUTID, F., MANGIN, R., SONNIER, R., SAEB, M. R., (2017), Novel nanocomposites based on poly (ethylene-co-vinyl acetate) for coating applications: the complementary actions of hydroxyapatite, MWCNTs and ammonium polyphosphate on flame retardancy. Progress in Organic Coatings, 113, 207-217.
30. WANG, X. F., HE, Z. Z., YANG, J. H., ZHANG, N., HUANG, T., WANG, Y., ZHOU, Z. W., (2016), Super toughened immiscible poly (L-lactide)/poly (ethylene vinyl acetate)(PLLA/EVA) blend achieved by in situ cross-linking reaction and carbon nanotubes. Composites Part A: Applied Science and Manufacturing, 91, 105-116.
31. YANG, C. J., HUANG, T., YANG, J. H., ZHANG, N., WANG, Y., ZHOU, Z. W., (2017), Carbon nanotubes induced brittle-ductile transition behavior of the polypropylene/ethylene-propylene-diene terpolymer blends. Composites Science and Technology, 139, 109-116.
32. YE, L., WU, Q., QU, B., (2009), Synergistic effects and mechanism of multiwalled carbon nanotubes with magnesium hydroxide in halogen-free flame retardant EVA/MH/MWNT nanocomposites. Polymer Degradation and Stability, 94(5), 751-756.
33. SUMITA, M., ASAI, S., MIYADERA, N., JOJIMA, E., MIYASAKA, K., (1986), Electrical conductivity of carbon black filled ethylene-vinyl acetate copolymer as a function of vinyl acetate content. Colloid and Polymer Science, 264(3), 212-217.
34. AZIZI, S., DAVID, E., FRÉCHETTE, M. F., NGUYEN-TRI, P., OUELLET-PLAMONDON, C. M., (2018), Electrical and thermal conductivity of ethylene vinyl acetate composite with graphene and carbon black filler. Polymer Testing, 72, 24-31.
35. SUJITH, A., UNNIKRISHNAN, G., (2005), Barrier properties of natural rubber/ethylene vinyl acetate/carbon black composites. Journal of materials science, 40(17), 4625-4640.
36. HUANG, J. C., WU, C. L., (2000), Processability, mechanical properties, and electrical conductivities of carbon black-filled ethylene-vinyl acetate copolymers. Advances in Polymer Technology: Journal of the Polymer Processing Institute, 19(2), 132-139.
37. FANG, Y., ZHAO, J., ZHA, J. W., WANG, D. R., DANG, Z. M., (2012), Improved stability of volume resistivity in carbon black/ethylene-vinyl acetate copolymer composites by employing multi-walled carbon nanotubes as second filler. Polymer, 53(21), 4871-4878.
38. ÇOPUROĞLU, M., ŞEN, M., (2005), A comparative study of UV aging characteristics of poly (ethylene-co-vinyl acetate) and poly (ethylene-co-vinyl acetate)/carbon black mixture. Polymers for advanced technologies, 16(1), 61-66.
39. ŞEN, M., ÇOPUROĞLU, M., (2005), A comparative study of gamma irradiation of poly (ethylene-co-vinyl acetate) and poly (ethylene-co-vinyl acetate)/carbon black mixture. Materials chemistry and physics, 93(1), 154-158.
40. SOARES, B. G., TOUCHALEAUME, F., CALHEIROS, L. F., BARRA, G. M., (2016), Effect of double percolation on the electrical properties and electromagnetic interference shielding effectiveness

of carbon-black-loaded polystyrene/ethylene vinyl acetate copolymer blends. Journal of Applied Polymer Science, 133(7).
41. DAS, N. C., CHAKI, T. K., KHASTGIR, D., (2003), Effect of filler treatment and crosslinking on mechanical and dynamic mechanical properties and electrical conductivity of carbon black-filled ethylene–vinyl acetate copolymer composites. Journal of applied polymer science, 90(8), 2073-2082.
42. MONDAL, S., KHASTGIR, D., (2017), Evaluation of carbon black distribution in different phases of compatible blend of EVA/NBR through electrical, mechanical and morphological test. Polymer Testing, 59, 404-413.
43. LU, H., LI, Z., QI, X., XU, L., CHI, Z., DUAN, D., ... DONG, Y., (2021), Flexible, electrothermal-driven controllable carbon fiber/poly (ethylene-co-vinyl acetate) shape memory composites for electromagnetic shielding. Composites Science and Technology, 207, 108697.
44. STAN, F., STANCIU, N. V., FETECAU, C., (2017), Melt rheological properties of ethylene-vinyl acetate/multi-walled carbon nanotube composites. Composites Part B: Engineering, 110, 20-31.
45. WANG, Y., LI, X., HOU, Y., QUAN, Y., YIN, C., YIN, Z., (2021), Stretchable and compressible conductive foam based on Cu nanowire/MWCNT/ethylene-vinyl acetate composites for high-mass-loading supercapacitor electrode. Chemical Engineering Journal, 417, 129176.
46. ZHANG, Z., WANG, W., LI, C., WEI, L., CHEN, X., TONG, Y., ... LU, X., (2014), Highly conductive ethylene-vinyl acetate copolymer/carbon nanotube paper for lightweight and flexible supercapacitors. Journal of Power Sources, 248, 1248-1255.
47. STAUFFER D, AHARONY A, REDNER S., Introduction to Percolation Theory[J]. Physics Today, 1987, 40(4):64-64.
48. DUAN, LINGYAN, et al. The resistivity-strain behavior of conductive polymer composites: stability and sensitivity. Journal of Materials Chemistry A, 2014, 2.40: 17085-17098.
49. ZHANG, X. W., PAN, Y., ZHENG, Q., YI, X. S., (2000), Time dependence of piezoresistance for the conductor-filled polymer composites. Journal of Polymer Science part B: polymer physics, 38(21), 2739-2749.
50. NATARAJAN, T. S., ESHWARAN, S. B., STÖCKELHUBER, K. W., WIEßNER, S., PÖTSCHKE, P., HEINRICH, G., Das, A., (2017), Strong strain sensing performance of natural rubber nanocomposites. ACS applied materials & interfaces, 9(5), 4860-4872.

Manuscript received: 16.08.2022